

GINS2 Functions as a Key Gene in Lung Adenocarcinoma by WGCNA Co-Expression Network Analysis

This article was published in the following Dove Press journal:
OncoTargets and Therapy

Wen Tian^{1,2}
Xianglin Yang^{1,2}
He Yang^{1,2}
Baosen Zhou^{1,2} 

¹Department of Clinical Epidemiology, First Affiliated Hospital, China Medical University, Shenyang, People's Republic of China; ²Department of Epidemiology, School of Public Health, China Medical University, Shenyang, Liaoning 110001, People's Republic of China

Background: Lung adenocarcinoma is one of the malignant tumors in the world. This study aimed to explore the biological mechanism of *GINS2* in lung adenocarcinoma.

Materials and Methods: Raw data were downloaded from GEO. WGCNA co-expression network and PPI network were established to identify the hub gene. The expression profile and clinical features of *GINS2* were collected from TCGA-LUAD cohort. Survival analysis in TCGA-LUAD cohort was plotted by R package. GSEA was analyzed via GSEA software. MTS, Transwell and apoptosis assays were used to detect the proliferation, migration and apoptotic abilities of lung adenocarcinoma cells.

Results: *GINS2* was identified as the hub gene via WGCNA co-expression network and PPI network. Higher *GINS2* expressions were observed in TCGA-LUAD cohort, GSE32863 and clinical samples dataset. Overexpression of *GINS2* had a significantly negative connection with poor survival outcome. GSEA results revealed that *GINS2* could be enriched in “HALLMARK_G2M_CHECKPOINT”, “HALLMARK_E2F_TARGETS”, “HALLMARK_DNA_REPAIR” and “HALLMARK_MYC_TARGETS_V2”. Overexpression of *GINS2* promoted tumor cell proliferation and migration and suppressed cell apoptosis.

Conclusion: Our results explored that *GINS2* functioned as an oncogene in lung adenocarcinoma, and suggested that *GINS2* could act as a promising prognosis biomarker for lung adenocarcinoma.

Keywords: *GINS2*, lung adenocarcinoma, WGCNA, biological function

Introduction

Lung cancer is one of the most prevalent cancers in the world, with 226,160 new cases and 160,340 mortalities in 2012.¹ Lung adenocarcinoma is a major subtype of lung cancer.² Due to the complex pathomechanism, the survival rate of lung adenocarcinoma is still low.³ Therefore, it is important to explore the underlying molecular mechanisms for lung adenocarcinoma development and progression.

GINS complex subunit 2 (*GINS2*), a member of *GINS* family, plays a crucial role in DNA duplication.⁴ In acute promyelocytic leukemia, up-regulation of *GINS2* facilitated HL60 cell proliferation.⁵ Down-regulation of *GINS2* inhibited breast cancer cells growth by activation of endogenous DNA damage.^{6,7} Elsewhere, it was found that deregulated *GINS2* expression promoted distant metastasis free survival and endocrine therapy resistance in breast cancer patients.⁸ A previous study has reported that *GINS2* mRNA was found to be significantly up-regulated in stage II lung adenocarcinoma.⁹

Correspondence: Baosen Zhou
Puhe Road, Shenyang, Liaoning 110012,
People's Republic of China
Email bszhou@cmu.edu.cn

In this research, we identified a novel oncogene, *GINS2*, in lung adenocarcinoma based on GSE32863 dataset. Additionally, we found that up-regulation of *GINS2* had better diagnostic values in lung adenocarcinoma. Notably, over-expression of *GINS2* promoted lung adenocarcinoma cells proliferation and migration and inhibited apoptosis in vitro.

Materials and Methods

Data Collection and DEGs Identification

GSE32863 contained 58 lung adenocarcinoma and 58 adjacent non-tumor lung fresh frozen tissues. The gene expression profile of GSE32863 was downloaded. Raw data was normalized by GEO2R calculation. Adjusted $p < 0.05$ and $|\log_2FC| > 1$ were set as the criterion for DEGs. The RNA sequencing and clinical data of lung adenocarcinoma were downloaded from TCGA database (<http://cancergenome.nih.gov/>). A total of 106 clinical samples from the case-control study were collected to analyze the relationship between *GINS2* expression and clinical information. All patients were informed of the study and provided written informed consent. The experiment was approved by the Institutional Review Board of China Medical University (No.67 in 2010) and conducted using methodologies conforming to the standards set by the Declaration of Helsinki.

Construction of WGCNA Co-Expression Network

The WGCNA was performed to construct a co-expression network of DEGs via R (3.6.2) WGCNA package. The soft threshold was determined when scale-free $R^2 > 0.85$. Then the cluster dendrogram and network heatmap of genes were constructed. In addition, eigengene values of modules were calculated, and a clustering tree was carried out.

KEGG and PPI Network Analyses

In order to explore the biological functions of cancer-associated genes, KEGG enrichment was analyzed via R *ggplot2* package. PPI network helps us to explore novel molecular mechanism. STRING (<https://string-db.org/>) online database is a tool to search the interaction among different proteins. The significantly associated genes with weight value > 0.8 were collected to construction PPI network.

Real Time-Polymerase Chain Reaction

Total RNA from cells was isolated by the reagent (Takara 9108, Takara, Japan). Then RNA was retro-transcribed according to the manufacturer's instructions (Takara RR047A, Takara, Japan). RT-PCR was performed by the SYBR Green PCR kit (Takara, Japan). PCR amplification was performed in triplicate according to Takara RR820A (Takara, Japan) under the conditions of 95°C for 30 and 40 second cycles at 95°C for 5 seconds and 60°C for 34 seconds. The Ct values were calculated via ABI 7500 Fast Real-time PCR System (ABI, USA). Fold changes in *GINS2* were measured by the $2^{-\Delta\Delta CT}$ method. The sequences of primer probes were as follows:

GINS2: Forward: AACTCCGCACGAACCT
Reverse: CCACGAGTACCTCATCAG

Western Blot

First, 20 μ L proteins were separated by 10% SDS-PAGE (Beyotime, People's Republic of China) and then transferred onto 0.45 μ m PVDF (Millipore, USA) membranes. After blocking with skim milk (BD 232100, BD, USA), the membranes were incubated overnight at 4°C with anti-*GINS2* (Abcam 37683, Abcam, People's Republic of China) and anti-*GAPDH* (Abcam 8245, Abcam, People's Republic of China) antibodies. Then membranes were incubated with a horseradish peroxidase-conjugated secondary antibody (Abcam 150117, Abcam, People's Republic of China) for 1 hour. The signal was detected with enhanced chemiluminescence (Thermo Scientific™ 34076, USA).

Cell Culture and Transfection

HBE and A549 were purchased from GeneChem (Shanghai, People's Republic of China). HBE and A549 cells were all cultured in RPMI-1640 (GIBCO, USA). All cell lines were maintained at 37°C in a humidified chamber with 5% CO₂. *GINS2* overexpression plasmid (OE-*GINS2*) and negative control plasmid (NC) were all purchased from Syngeneiech (Beijing, People's Republic of China). 1×10^5 to 1.5×10^5 cells were seeded into 6-well plates and transfected plasmids using jetPRIME transfection reagent (Polyplus transfection, USA) according to the manufacturer's instructions. After being transfected for 48 hours, all cells were collected and used for the next experiments. The sequences of all plasmids were as follows:

OE-*GINS2*: 5'-GGATCCCGAAGGCAGACGA-3'
NC: 5'-TTCTCCGAACGTGTACCGT-3'

Cell Growth

A total of 1×10^4 cells were collected and seeded into 96-well plates. The cell growth was measured with MTS solution (Promega G3580, People's Republic of China) according to the instructions. Cells were incubated at 37°C for 2 hours, adding 20 μL MTS solution. The OD was assessed at 0, 12, 24 and 48 hours at 490 nm. Each group was tested in five parallel samples.

Cell Apoptosis

Transfected cells were seeded in a 6-well plate. And then cells were collected by trypsin digestion without EDTA (Thermo

Fisher, USA). The apoptotic rates of cells were estimated by Annexin V-APC/7-AAD (KGA1016, KeyGen BioTECH, People's Republic of China) according to the protocols. Cells were stained with 5 μL 7-Amino-Actinomycin D and 5 μL Annexin V-Allophycocyanin at 37°C for 10 minutes. The cells were detected by FCM (Merck Millipore, Germany).

Cell Migration

Transfected cells were starved for 48 hours. Then cells (1×10^4) were resuspended in 200 μL serum-free medium, and seeded in the top chamber with 8.0 μm pores in the membrane (Corning, NY, USA). Culture medium with

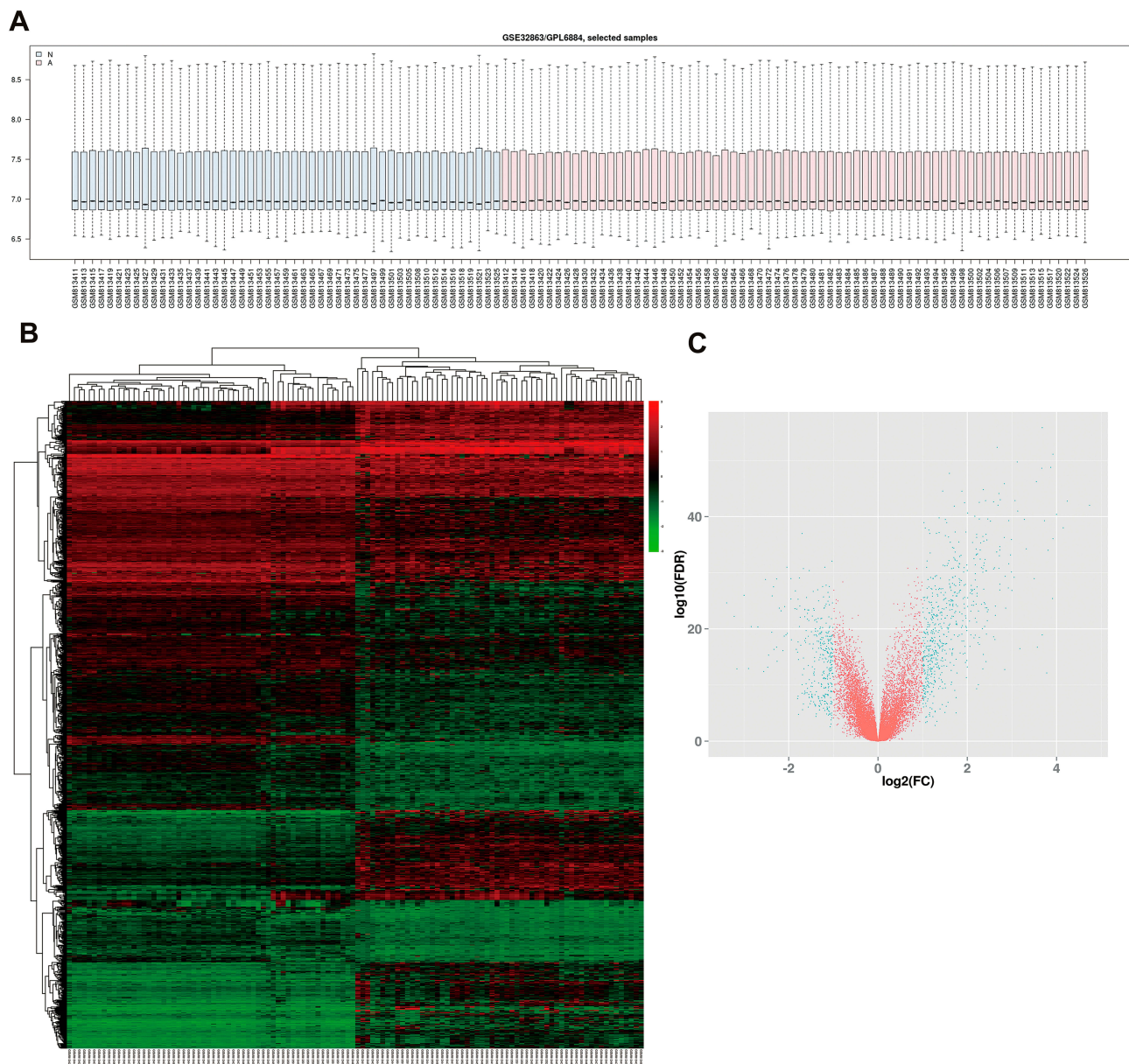


Figure 1 Identification of DEGs in GSE32863 dataset. (A) Normalization of GSE32863 data. (B) Heatmap of all genes expression in GSE32863. (C) The volcano map of DEGs.

Table I The Differently Expressed Genes in GSE32863

	Number	Gene Names
Down-regulated genes	339	<p> <i>SPP1, GCNT3, SPINK1, MMP11, EEF1A2, CRABP2, COL1A1, CST1, CEACAM5, TOP2A, COMP, TUBB3, SLC2A1, PROM2, ITPKA, MMP9, SERINC2, PITX1, CDC20, SFN, HMGB3, FAM83A, C1orf106, CDH3, ETV4, PODXL2, GPT2, KRT8, SPDEF, TK1, SEMA4B, MUC20, SBK1, CTHRC1, LCN2, GSDMB, HOOK1, LMOD3, S100P, SLC29A4, OCLAD2, TMEM45B, CHPF, CDC45, THBS2, CHMP4B, MAGT1, MUC21, GPX2, NQO1, BAIAP2L1, DSP, ITCH-IT1, CLDN3, USP49, AGRN, METTL7B, TNFRSF211, UHRF1, ZNF69, HSD17B7, FUT3, XPR1, SCG5, SLC16A3, TIMP1, ZNF14, PAFAH1B3, ST14, WDR66, ERO1A, CDCA7, CELSR3, CXCL14, ALPP, MARCKSL1, TTYH3, BLZF1, COL3A1, PPP1R14B, SSTR2, PFKF, PCP4, TESC, AOC4P, BCRYN1, CCNB2, ATP10B, PC, CAPN8, DUSP19, NUBPL, ZNF786, AURKA, SLC7A5, VSTM2L, YRDC, TMPRSS4, DDR1, KRT80, FAM83H, HIST1H2BD, LRRFIP1, COL5A2, 6-Mor, RHOD, STX1A, HES6, MAPK8IP3, PCSK1N, PRC1, RGS17, TUBB2B, CFB, MBD4, PTGR2, SPC24, CCNF, MCM4, TCN1, COL10A1, SLC25A51, TM4SF4, CDH1, PAICS, FUT2, NUSAP1, P3H4, SLC39A11, ADAM8, GALNT3, GINS2, IGFBP3, JUP, NMU, RRBPI, ZNF652, MGRN1, MUC16, STK39, CRLF1, ZNF223, CEACAM6, ELF3, PGHGH, TLCD1, UBE2T, AURKB, GLB1L2, MCM2, SLC22A18AS, SOX4, TDRD1, ANKRD22, TMEM132A, TMEM54, CAPN12, CERCAM, SLC4A5, SRPX2, SULF1, AGR2, AOCI, ASPM, F12, PDIA4, PHLDA2, ITPK1-AS1, RASEF, ARFGAP1, KCNK5, PSAT1, SIX4, SRPK1, CENPF, MX2, TXNDC17, ZNF486, CDC45, DEAF1, FAM63A, NRIP3, SORD, ZNF750, CNFN, IGF2BP3, PLOD2, SAPCD2, SCIN, SLC52A2, TRIM2, ABCA4, ARHGEF19, GNL3L, ST6GALNAC1, STIL, AHNAK2, CA9, KDELR2, KDM5B, MBTD1, SLC5A8, AIM2, ARHGAP39, CANT1, DNAH2, ECT2, EIF2AK4, KCNK1, COL5A2, ABCB6, HABP2, SLC16A9, WSB1, BOP1, CERS6, DBNDD1, E2F2, NARF, VARS, BAIAP2L2, FAM13A, GDF15, H1FO, FAM234A, HAUS2, HKDC1, LOC105375172, THY1, VWA1, FHL2, LDHA, MMP15, NPM3, PCDHB19P, PTGES, RAX2, REEP6, SMPDL3B, XKRX, CNOT11, GOLGA8A, HIST2H2AC, IGSF9, PSG1, RAB25, COL9A2, GALNT6, GFRA3, ITGA2, KIAA1, KIFC1, MRPL12, PA2G4, PLEK2, RHPN2, SPSB1, TSTA3, ALG1L, BRI3BP, ELMO3, FOXA3, NET1, SLC50A1, ATAD3A, BZW2, HACD4, ENCI, KIAA1522, KIF20A, KRT15, P4HB, PANX2, PPM1K, RMI2, CLPTM1L, H2AFX, HYOU1, LAPTM4B, PTPRF, PTTG3P, FGFR1, GFPT1, GPR37, JSRPI, TFF1, GCAT, GJB2, ISG15, KCNK12, KISS1R, PDIA6, IL37, SERPINH1, SHMT2, SPIRE2, ACOT11, CLDN2, DDIT4L, DDX27, IDH2, KRT17, MST1R, PLXNA3, PRRC2A, PSME4, TMEM106C, TRIP13, ZNF827, DCBLD1, DHRS11, DPP9, FOXQ1, IRAK1, KRT19, BCAS4, TMEM63A, AKR1B10, CCDC34, DNTTIP1, FAM83E, KNTC1, MESPI, POC1A, SAC3D1, TAOK1, TNFRSF12A, TYMS, UBE2O, C17orf53, CHTF18, MTA3, SDHAP3, TIMELESS, TMEM62, TPX2, ALDH18A1, ENO2, L2HGDH, LRRC20</i> </p>
Up-regulated genes	628	<p> <i>LOC401286, MCEMP1, HBB, CA4, HBA2, ITLN2, FCN3, FAM107A, HBA1, SCGB1A1, ADH1A, FABP4, SFTPC, CLEC3B, PGC, CAV1, GKN2, INMT, MFAP4, FOSB, GPIHBP1, FMO2, PLAC9, TMEM100, MARCO, ADIRF, CCL14, CFD, CRTAC1, SPOCK2, MTIM, S100A8, PEBP4, ITLN1, AGER, CAV2, RGCC, ACKR1, CPA3, MAMDC2, SEPP1, SDPR, CD52, LDB2, LYVE1, ADH1B, SPARCL1, GNG11, IL6, CYP4B1, TNNC1, CLDN5, PLA2G1B, TEK, HIGD1B, C7, FHL1, PRG4, PTGDS, DCN, SVEP1, HSD17B6, PCOLCE2, ANOS1, CDH5, SFTPD, ABCA8, OLR1, CACNA2D2, VSIG4, CLIC5, CPB2, DNASE1L3, ITM2A, LAMP3, TIMP3, SLPI, STX11, CLEC14A, FCN1, LYZ, MS4A7, CXCL2, IL33, ALOX5AP, GPC3, CD93, PGM5, SRPX, MME, PECAM1, SOX18, WIFI, C9orf24, EFEMP1, CA2, VWF, C2orf40, FPR1, MGR, ABI3BP, COX7A1, CRYAB, SCGB3A2, SMAD6, C1orf162, PDK4, TGFBR3, PI16, SEMA6A, SRGN, TPSAB1, TSPAN7, MMRN1, LPL, ALDH1A1, EPAS1, AGRP, ID3, GLIPR2, SOSTDC1, GPX3, COLEC12, HBEGF, HOXA5, JAM2, ADAMTS1, S100A4, DUOX1, TSC22D1, TYROBP, CD163, CYR1, FBLN1, ADRB2, SUSD2, MYH11, VIPR1, WNT3A, ALPL, IL7R, CIQA, FCERIA, GYPC, ZFP36, AQP1, CALCR1, SLC39A8, ACTG2, CTSG, AIF1, CCM2L, DPT, CAMP, PPP1R14A, RASIP1, ANGPT1, SLC6A4, FOLR3, RAMP3, FCER1G, CYBRD1, GAS1, S100A3, GIMAP4, RETN, FBLN5, CGNLI, CCL2, FAM189A2, AQP9, CAT, ESAM, FAM150B, PLA2G4F, SCARAS, BTG2, GIMAP5, HSPB8, SLC31A2, FGD5, P3H2, HSPA12B, RASL12, ABCA3, ID2, WISP2, DUSP1, LTC4S, TGFBR2, GLDN, C4BPA, CLIC3, ENPP2, LRRC32, LTBP4, SCGB3A1, SLIT2, EVI2B, TACCI1, CPED1, HEG1, PTPRB, SLC19A3, TMEM74B, ID1, ACVRL1, CD302, VSIG2, ALDH1A2, PDI1, PPP1R15A, S1PR1, DPEP2, EMCN, STOM, FXDY6, KLF2, CCL21, GMFG, JAML, LMO2, SASH1, TOX2, AP1S2, COL6A6, CSRNPI, FZD4, LHFP, CIQB, EGR2, TCEAL2, ARHGEF6, CLEC1A, GJC2, ARHGAP44, CXCL12, GDF10, ANXA3, NOSTRIN, OLFML1, C10orf54, JCHAIN, LIMCH1, FMO3, PTPRM, SOCS2, SOX7, CXCR4, KLF9, LIMS2, NDN, TMEM204, FAM183A, GIMAP7, KANK2, LY86, VIM, ADAMTS8, CESIP1, CRTAP, CTNNA1, EMP3, KANK3, ZNF385B, CD300LF, KLK11, MS4A2, MS4A6A, TEKTI1, FCGR1B, HBG2, MYH10, PROS1, SLCO2B1, GSTM3, IL1B, PPM1F, STXB6, SNCA, SPON1, CCND2, FCGR2A, HSPB6, MS4A15, MTIX, RHOJ, SGCE, C1orf88, FAM216B, FAM65A, HP, IFI30, LAMC3, SBSPO, GADD45B, GBP4, HSPC324, SIRPA, SLC15A3, SOCS3, ROPN1L, RPL13AP17, COX4I2, LPXN, MAP3K8, SLCO2A1, SLIT3, CSAR1, MT2A, NCF1, DOCK2, EFCAB1, S100A9, SERPING1, SPARC, ZBED2, CYB5A, DAB2, FAM167A, FAM212A, NKG7, ACKR3, DPYSL2, GHR, HBG1, PDPN, TCF21, DUOX1, FERMT2, FGR, HLA-DRB3, IGFBP7, OSCAR, A2M, CD37, ICAM2, IFT57, AHNAK, BTK, CPVL, PTH1R, RNF144B, SESN1, ANKRD1, COL13A1, F13A1, METTL7A, PLEK, ADCY4, HLA-DRB6, PDLIM3, PLLP, CHPT1, GJA4, HSPB2, LAMA4, MTURN, SYT15, ADGRE5, C1orf21, CTGF, EMP1, FIGF, LCPI, LMO7, MAF, AGR3, C1orf115, EFEMP2, EGR1, EPB41L2, LGI3, MNDA, DES, MSLN, NDNF, SERPINA3, TRPV2, VNN2, WFS1, CIQC, ETS1, C6, GFGBP2, GSTA4, HCST, SLC2A3, ARMXC1, ETS2, FGL2, HLA-DPA1, LILRB3, SNURF, ALDH2, CYBB, CYR61, EML1, LUM, MAOB, CBX7, HCK, IRF8, LRRN3, PRKCH, SELENBP1, ZFP36L2, C1orf186, CH25H, CNN1, HPGD, TFRC, WFDC1, AVPI1, CD33, DENND2A, FCGR3B, KLRB1, LYLI, PAPSS2, PRKCDBP, TLR8, TSPAN32, UBL3, ZNF106, AADAC, ACP5, AK1, APOL3, C10orf67, CD53, GRASP, HEY1, NR4A2, OLFML2A, PTGIS, RAMP2, RNASE4, TUBB6, UBB, APOLD1, JUN, CD300C, CD83, ENG, ITPRI, KLF13, LDLR, NPNT, PPP1R3C, RAB8B, CDO1, CHMP3, HLA-DRA, LRRK2, LST1, SGK1, SH3BGRL, SLC46A2, ACADL, ACSL4, GLIPR1, SOST1, GZMH, LAPTM5, TBX2, ADGRL2, CNRIP1, KCNJ8, MATN2, MS4A8, NKD2, SECISBP2L, WASF3, FOLR1, FOLR2, MTIG, P2RY3, SBDSP1, SCN4B, SH3GL3, CAMK2N1, EPB41L3, FBPI, FGGY, GABARAPL1, GATA2, NOTCH4, AAMDC, CLEC12A, FGD3, GFOD1, LILRA2, MTIA, SOX17, TM6SF1, KLF6, RAB11FIP1, SNRPN, TUBA1A, BORCS7, C1orf198, CCL3, CIRBP, EMILIN2, FAM43A, MAL, NINJ2, RPL17, TMEM88, UBE2E2, ANXA2, ARAP3, CD14, HCLS1, HDC, NCF1C, PRX, RTKN2, SDCBP, TSPAN18, ZYX, AOC3, DYNLRB2, HHIP, HLA-DQB1, MSRA, NUPR1, SH2B3, ZEB2, CRBN, CXCL8, DOCK11, RGS5, SPI1, AOX1, ATOH8, C2, CCDC178, CD59, MYOM2, PAMR1, ACTG1, CALB2, CAPS, EDN1, GCHFR, PHACTR2, STARD8, UBE2L6, C8B, EIF1B, GNG10, GSTM5, MAOA, PRICKLE2, C3, CD9, DLL1, GPRC5A, HSD17B11, MSR1, RBP1, SEC22C, ANG, FLNC, FPR2, GALNT18, PLIN2, TMEM140, TNFRSF19, TSPAN4, VGLL3, DACT3, F10, H3F3B, INAFM1, JUNB, MTIE, S1PR4, SELE, ZNF331, ANO6, APOC1, AXIN2, BTG1, GJA1, IFNGR1, IL17D, NEDD4L, PPP1R16B, QDPR, REM1, TMOD1, TMSB15A, ADTRR, CCL18, CDH13, CDHR3, FGFR4, IRF1, LXN, RCANI, RERG, RPL21, TNS3</i> </p>

10% FBS was added to the bottom chamber. After 48 hours at 37°C, the cells in the top chamber were immobilized with paraformaldehyde for 15 minutes and then stained with crystal violet (0.1%) for 10 minutes. After washing with double-distilled water three times, the chamber was stained with 0.1% the crystal violet. After drying, the number of cells migrating was counted by an inverted microscope (ECHO, CA, USA).

Statistical Analysis

The overall survival (OS) were analyzed via R survival package. Student's test was performed to validate *GINS2* expression differences between different groups via R ggplot2 package. Two-way analysis of variance was conducted to analyze the difference in cell growth between the

two groups. A two-sided $p < 0.05$ was considered statistically significant.

Results

Identification of DEGs

In order to verify DEGs, we normalized the raw data of GSE32863 via GEO2R calculation (Figure 1A). The heatmap of all genes is shown in Figure 1B. Adjusted $p < 0.05$ and $|\log_2FC| > 1$ were set as the criterion of DEGs (Figure 1C), including 628 up-regulated genes and 339 down-regulated genes (Table 1).

WGCNA Co-Expression Network

Based on GSE32863 up-regulated genes expression, we constructed a WGCNA co-expression network. As shown

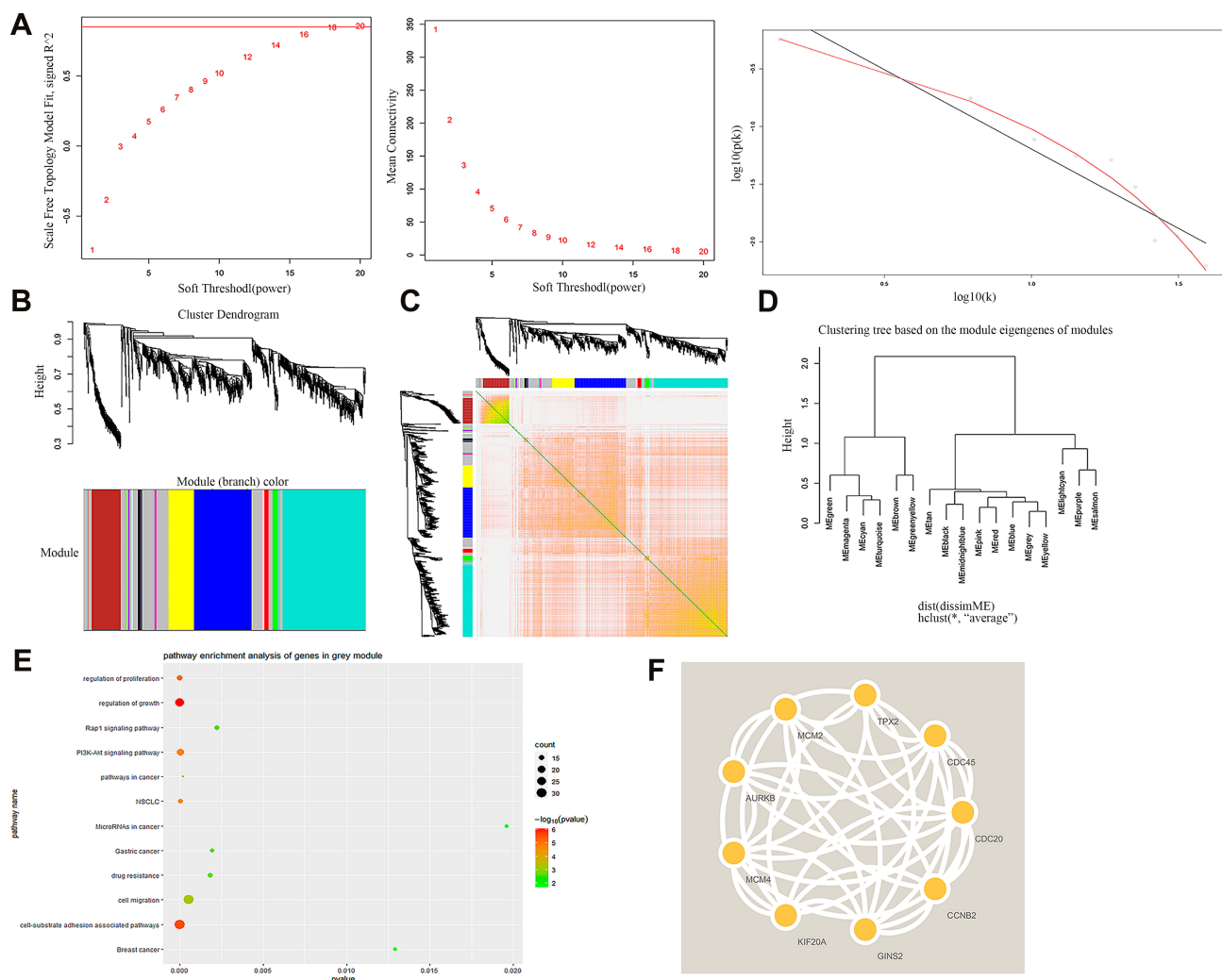


Figure 2 WGCNA co-expression network analysis of GSE32863. (A) Scale independence, mean connectivity and scale-free topology. (B) Cluster dendrogram of all up-regulated genes. (C) interaction relationship of co-expression genes. (D) Clustering tree based on the module eigengenes of modules. (E) KEGG analysis of genes in grey module. (F) PPI analysis of top nine up-regulated genes.

Table 2 Each Number of Each Module in WGCNA

Colour	Number	Gene Names
Black	3	<i>MTIX, MT2A, MT1A</i>
Blue	12	<i>C9orf24, C20orf85, FAM183A, TEK1, C11orf88, C6, FAM216B, ROPN1L, EFCAB1, MS4A8 CAPS, DYNLRB2</i>
Brown	5	<i>TYROBP, FCER1G, CIQA, CIQB, CIQC</i>
Green	3	<i>LDB2, CD93 CYYR1</i>
Grey	559	<i>SPP1, GCNT3, SPINK1, MMP11, EEF1A2, CRABP2, COL1A1, CEACAM5, TOP2A, CST1, COMP, DSP, CDH3, TUBB3, SLC2A1, PROM2, ITPKA, MMP9, SERINC2, PITX1, CDC20, SFN, HMGB3, ST14, FAM83A, C1orf106, ETV4, PODXL2, GPT2, KRT8, SPDEF, TK1, SEMA4B, MUC20, SBK1, CTHRC1, LCN2, GSDMB, HOOK1, S100P, SLC29A4, TIMP1, OCIAD2, TMEM45B, CHPF, CDCA5, THBS2, CHMP4B, MUC21, GPX2, NQO1, BAIAP2L1, CLDN3, AGRN, METTL7B, TNFRSF21, UHRF1, FUT3, XPR1, SCG5, SLC16A3, PAFAH1B3, PC, WDR66, ERO1A, CDCA, CELSR3, CXCL14, MARCKSL1, TTYH3, COL3A1, PPP1R14B, PFKP, PCP4, TESC, CCNB2, ATP10B, CAPN8, AURKA, SLC7A5, VSTM2L, TMRSS, DDR1, KRT80, FAM83H, HIST1H2BD, COL5A2, RHOD, STX1A, HES6, MAPK8IP3, PCSK1N, PRC1, RGS17, CFB, TUBB2B, SPC2, CCNF, MCM4, TCN1, COL10A1, TM4SF4, CDH1, PAICS, FUT2, NUSAP1, MCM2, SLC39A11, ADAM8, GINS2, IGFBP3, JUP, NMU, RRBPI, MGRN1, MUC16, STK39, CRLF1, ELF3, CEACAM6, PGGHG, TLCD1, UBE2T, AURKB, GLB1L2, SLC22A18AS, SOX4, ANKRD22, P3H4, TMEM132A, TMEM54, CAPN12, CERCAM, F12, SRPX2, SULF1, AGR2, AOCI, ASPM, PDIA4, MX2, PHLDA2, RASEF, ARFGAP1, KCNK5, PSAT1, SIX4, SRPK1, CENPF, TXNDC17, CDC45, DEAF1, NRIP3, SORD, ZNF750, CNFN, IGF2BP3, PLOD2, SAPCD2, SCIN, SLC52A2, TRIM2, CA9, ABCA4, ARHGGEF19, GNL3L, ST6GALNAC1, STIL, AHNAK2, KDELR2, KDM5B, AIM2, EZF2, ARHGAP39, CANTI, DNAH2, ECT2, KCNK1, ABCB6, HABP2, SLC16A9, BOPI, CERS6, NARF, DBNDD1, VARS, BAIAP2L2, FAM13A, GDF15, HIF0, FAM234A, HKDC1, LOC105375172, THY1, VWAI, FHL2, LDHA, MMP15, NPM3, PTGES, CA4, REEP6, SMPDL3B, XKRX, CNOT11, PSG1, GOLGA8A, HIST2H2AC, IGSF9, RAB25, KIF1A, COL9A2, GALNT6, GFRA3, ITGA2, KIFC1, MRPL12, PA2G4, PLEK2, RHPN2, SPSB1, TSTA3, ALG1L, BRI3BP, ELMO3, FOXA3, NET1, IDH2, SLC50A1, ATAD3A, BZW2, KIAA1522, KIF20A, KRT15, P4HB, PANX2, RMI2, CLPTM1L, ENCI, H2AFX, HYOU1, LAPTM4B, PTPRF, PTTG3P, FGFRL1, GFPT1, GPR37, JSRPI, TFF1, GCAT, GJB2, ISG15, KCNK12, KISS1R, PDIA6, IL37, SERPINH1, SHMT2, SPIRE2, ACOT11, CLDN2, DDIT4L, DDX27, KRT17, MST1R, PLXNA3, PRRC2A, PSME4, TMEM106C, TRIP13, ZNF827, DCBLD1, DHRS11, DPP9, FOXQ1, IRAK1, KRT19, TMEM63A, AKR1B10, CCDC34, DNTTPI1, CFD, FAM83E, KNTC1, MESPI, POC1A, SAC3D1, TAOK1, TNFRSF12A, TYMS, UBE2O, C17orf53, CHTF18, MTA3, SDHAP3, TIMELESS, TMEM62, TPX2, ALDH18A1, BCAS4, ENO2, L2HGDH, LRRC20, LOC401286, MCEMP1, HBB, HBA2, ITLN2, FCN3, FAM107A, HBA1, SCGB1A1, ADH1A, FABP4, SFTPC, PGC, CAV1, GKN2, INMT, MFAP4, FOSB, GPIHBP1, FMO2, PLAC9, TMEM100, MARCO, ADIRF, CCL14, CRTAC1, SPOCK2, MT1M, S100A8, PEBP4, ITLN1, AGER, CAV2, RGCC, ACKR1, CPA3, MAMDC2, SEPP1, SDPR, CD52, LYVE1, ADH1B, SPARCL1, GNG11, IL6, CYP4B1, TNNC1, CLDN5, PLA2G1B, C7, HIGD1B, FHL1, PRG4, PTGDS, DCN, SVEP1, HSD17B6, PCOLCE2, ANOS1, SFTPD, ABCA8, OLR1, CACNA2D2, VSIG4, CLIC5, CPB2, DNASE1L3, ITM2A, LAMP3, TIMP3, SLPI, STX11, CLEC14A, FCN1, LYZ, MS4A7, CXCL2, ALOX5AP, GPC3, PGM5, SRPX, MME, PECAM1, SOX18, WIF1, EFEMP1, CA2, VWF, C2orf40, FPR1, MGP, ABI3BP, COX7A1, CRYAB, SCGB3A2, SMAD6, C1orf162, PDK4, TGFB3, P116, SEMA6A, SRGN, TPSAB1, TSPAN7, MMRN1, LPL, ALDH1A1, AGRP, ID3, GLIPR2, SOSTDC1, GPX3, COLEC12, HBEGF, HOXA5, IL33, ADAMTS1, S100A4, DUOX1, TSC22D1, CD163, FBLN1, ADRB2, SUSD2, MYH11, VIPR1, WNT3A, ALPL, IL7R, FCER1A, GYPC, ZFP36, AQPI, CALCRL, SLC39A8, ACTG2, CTSG, AIFI, DPT, CAMP, PPP1R14A, RASIP1, ANGPT1, SLC6A4, FOLR3, RAMP3, CYBRD1, GAS1, JAM2, S100A3, GIMAP4, RETN, FBLN5, CGNL1, CCL2, FAM189A2, AQP9, CAT, ESAM, FAM150B, PLA2G4F, SCARAS, BTG2, GIMAP5, HSPB8, SLC31A2, FGD5, HSPA12B, RASL12, ABCA3, ID2, WISP2, DUSP1, LTC4S, P3H2, TGFB2, GLDN, C4BPA, CLIC3, ENPP2, LRRC32, LTBP4, SCGB3A1, SLIT2, EVI2B, TACCI, CPED1, HEG1, PTPRB, SLC19A3, TMEM74B, ACVRL1</i>
Red	3	<i>TEK, CDH5, EPAS1</i>
Turquoise	40	<i>LMOD3, MAGT1, ITCH-IT1, USP49, ZNF69, HSD17B7, ZNF14, ALPR, BLZF1, SSTR2, AOC4P, BCYRN1, DUSP19, NUBPL, ZNF786, YRDC, LRRFIP1, 6-Mar, MBD4, PTGR2, SLC25A51, GALNT3, ZNF652, ZNF223, TDRD1, SLC4A5, ITPK1-AS1, ZNF486, FAM63A, MBTD1, SLC5A8, EIF2AK4, WSB1, HAUS2, PCDHBI9P, RAX2, HACD4, PPM1K, CHMP3, GNG10</i>
Yellow	3	<i>CLEC3B, CCM2L, COX4I2</i>

in Figure 2A, the soft threshold of $\beta=18$ was identified ($R^2=0.9$, slope=-1.38). Then, all up-regulated genes were split into eight modules (Figure 2B). Each module had different color and genes (Table 2). Figure 2C plotted the network heatmap of interaction of eight modules. All the modules were significantly independent of each other, and a similar result was also observed in gene expressions in each module. In addition, eigengene module values were

calculated in each module and a clustering tree is presented in Figure 2D.

Among all the modules, the grey module had the highest number of genes, containing 559 up-regulated genes. KEGG results indicated that those highly expressed genes were mainly enriched in regulation of growth, cell migration and cell-substrate adhesion associated pathways (Figure 2E). Then we constructed a PPI network to further

identify the hub gene. The PPI network of the top nine genes is presented in Figure 2F. Table 3 shows that *GINS2* in the grey modules had the highest score (score=0.999). Herein, we explored the biological function of *GINS2* in lung adenocarcinoma.

Expression and Clinical Value of *GINS2* in Lung Adenocarcinoma

Figure 3A shows that the expressions of *GINS2* in patients from the TCGA-LUAD cohort, GSE3286 and clinical samples dataset were significantly higher than that in healthy controls (TCGA-LUAD cohort: $p < 0.001$; GSE32863: $p < 0.001$; clinical samples dataset: $p < 0.001$). Overexpression of *GINS2* in the TCGA-LUAD cohort was strongly associated with poor prognosis (Figure 3B: $p = 0.0075$). Next, we performed the ROC curve to establish the prognostic ability of *GINS2* in the TCGA-LUAD cohort (Figure 3C), GSE32863 (Figure 3D) and clinical samples dataset (Figure 3E). Table 4 shows that the AUCs of *GINS2* in the TCGA-LUAD cohort, GSE32863 and clinical samples dataset were 0.847 ($p = 0.0023$), 0.894 ($p < 0.001$) and 0.851 ($p < 0.001$), respectively. Combined with high sensitivity and specificity, *GINS2* could be considered as a candidate prognostic biomarker in lung adenocarcinoma. In addition, GSEA results revealed that high *GINS2* expression in the TCGA-LUAD cohort was significantly enriched in the gene sets of “HALLMARK_G2M_CHECKPOINT”, “HALLMARK_E2F_TARGETS”, “HALLMARK_DNA_REPAIR” and “HALLMARK_MYC_TARGETS_V2” (Figure 3F). The results further suggest that *GINS2* plays a vital role in the prognosis of lung adenocarcinoma.

We also explored the relationship between *GINS2* expression and clinical information. As Table 5 illustrates, in the clinical samples dataset, *GINS2* expression is significantly related to the clinical stage ($p < 0.001$), but not with age, gender or smoking status.

Effects of *GINS2* on Growth, Migration and Apoptosis of Tumor Cells

The results of RT-PCR (Figure 4A) and Western blot (Figure 4B) showed that the expression of *GINS2* in A549 cells was significantly up-regulated. Then we transfected OE-*GINS2* and NC plasmids to A549 cells to explore biological functions of *GINS2*. Expression levels of *GINS2* in cells transfected with blank, NC and OE-*GINS2* were estimated by PCR (Figure 4C) and Western blot (Figure 4D). *GINS2* expression was significantly over-expressed in cells transfected with OE-*GINS2* ($p < 0.001$). The result of the MTS assay showed that the growth rate was significantly increased in cells transfected with OE-*GINS2* (Figure 4E: $p < 0.001$), suggesting that up-regulation of *GINS2* had a significant promotion effect on lung adenocarcinoma cells proliferation. In addition, Figure 4F showed that the migration viability of cells transfected with OE-*GINS2* was significantly increased compared with cells transfected with NC and blank ($p < 0.001$). Figure 4G showed that the apoptosis rate of tumor cells with *GINS2* overexpression was significantly decreased. No significant differences between NC and blank groups were observed.

Discussion

The pathomechanism of lung adenocarcinoma is complicated and multifaceted. Numbers of oncogenes or tumor suppressor genes had been proved in the occurrence and progression of lung adenocarcinoma. In our study, we systematically analyzed the oncogene role of *GINS2* in lung adenocarcinoma.

Initially, we analyzed the raw data in GSE32863 and 967 DEGs were identified. Next, we constructed a WGCNA co-expression network to classify DEGs into different modules. WGCNA is a systematic approach to dividing genes with similar expression patterns into the

Table 3 Nine Hub Genes in the PPI Network Constructed by STRING

Gene Names	Description	Score
<i>CDC20</i>	Cell division cycle 20	0.999
<i>CDC45</i>	Cell division cycle 45	0.999
<i>GINS2</i>	GINS complex subunit 2	0.999
<i>MCM2</i>	Minichromosome maintenance complex component 2	0.998
<i>MCM4</i>	Minichromosome maintenance complex component 4	0.998
<i>CCNB2</i>	Cyclin B2	0.997
<i>AURKB</i>	Aurora kinase B	0.997
<i>KIF20A</i>	Kinesin family member 20A	0.996
<i>TPX2</i>	TPX2 microtubule nucleation factor	0.995

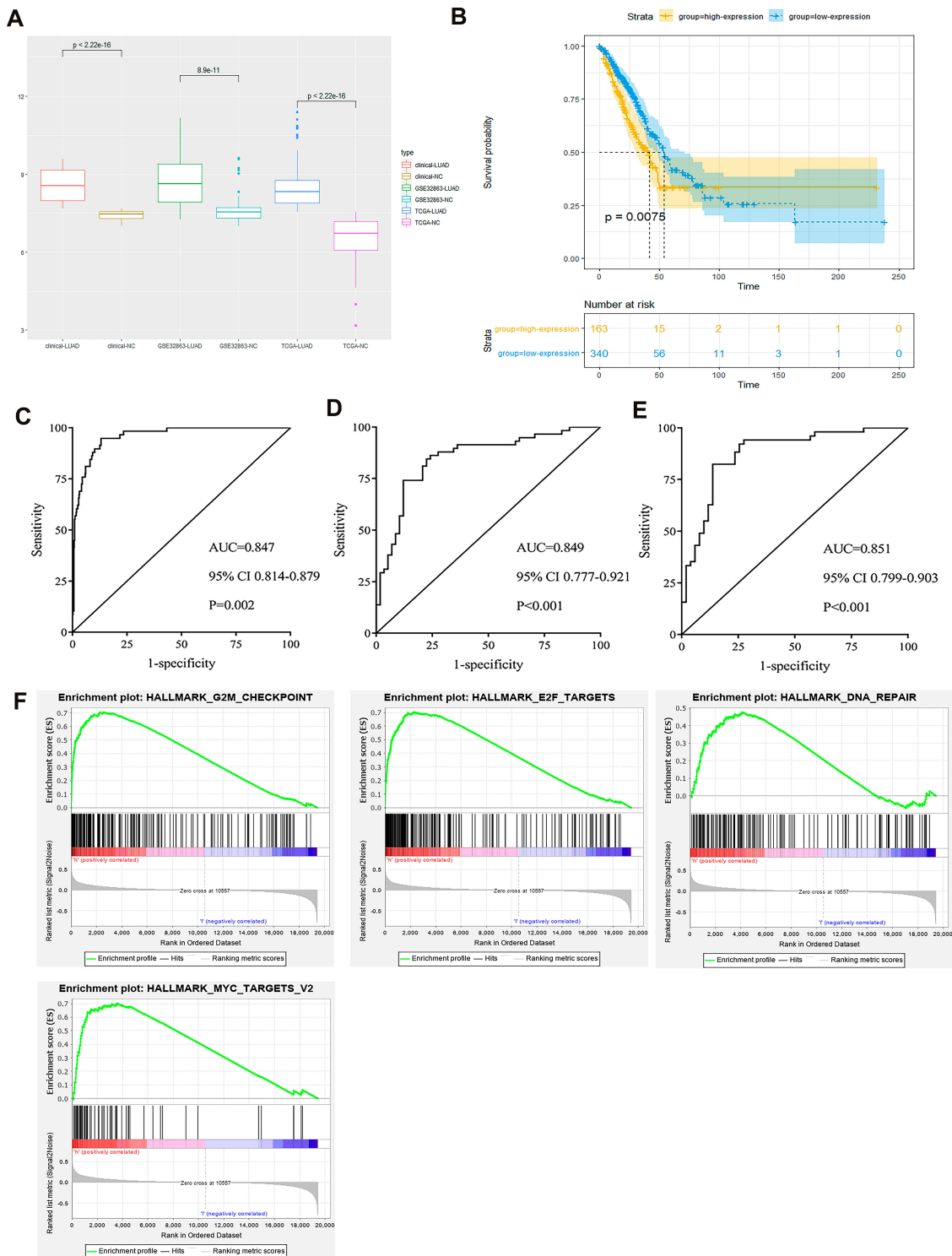


Figure 3 Integrative analyses of *GINS2*. **(A)** *GINS2* expression in TCGA-LUAD cohort, GSE32863 and clinical samples dataset. **(B)** Prognostic analysis of *GINS2* in TCGA-LUAD cohort. **(C–E)** ROC analysis of *GINS2* in TCGA-LUAD cohort **(C)**, GSE32863 **(D)** and clinical samples dataset **(E)**. **(F)** GSEA analysis results of *GINS2*.

same modules and further exploring correlation between modules.^{10,11} In our study, after identifying the key module, pathway prediction results illustrated that those genes were mainly enriched in regulation of growth, regulation

of cell proliferation and substrate adhesion pathways, suggesting that those DEGs may participate in the occurrence and development of lung adenocarcinoma. In addition, we constructed a PPI network to further identify the hub gene

Table 4 ROC Analyses Results of GSE32863, TCGA and Clinical Samples

Dataset	AUC	95% CI	Sensitivity	I-Specificity	P-value
GSE32863	0.894	0.777–0.921	0.983	0.862	<0.001
TCGA-LUAD	0.847	0.814–0.879	0.996	0.817	0.0023
Clinical samples	0.851	0.799–0.903	0.987	0.883	<0.001

Table 5 The Relationship Between *GINS2* Expression and Clinical Features in Our Case-Control Study

Variables		<i>GINS2</i> Expression Level		χ^2	P-value
		Low (n=62)	High (n=44)		
Age (years)	<60	11	10	0.399	0.528
	≥ 60	51	34		
Gender	Male	14	9	0.068	0.794
	Female	48	35		
Smoking statue	No	33	19	1.039	0.308
	Yes	29	25		
Clinical stage	I+II	49	11	30.588	<0.001
	III+IV	13	33		

in the grey module. *GINS2*, with the highest score, was selected to explore the molecular mechanism in lung adenocarcinoma.

Based on the heterotetramer complex structure, *GINS2* plays a vital role in chromatin binding and replication activity.¹² In other human tumors, for example, in thyroid cancer, over-expression of *GINS2* activated cancer cells proliferation and inhibited apoptosis by mediating *CITED2* and *LOXL2*;^{13,14} In early-stage cervical cancer, *GINS2* was significantly over expressed in tumor tissues and cancer cells and had a negative correlation with OS of cervical cancer patients.¹⁵ In our study, we downloaded *GINS2* expression profile and clinical characteristics in TCGA-LUAD cohort. Over-expression of *GINS2* was observed in the TCGA-LUAD cohort, GSE32863 and clinical samples dataset. Additionally, aberrant expression of *GINS2* was significantly associated with poor prognosis in lung adenocarcinoma patients. ROC analysis results showed the higher diagnostic value of *GINS2* in lung adenocarcinoma. Besides, we concluded that aberrant *GINS2* expression had a significant correlation with lung adenocarcinoma clinical stage. Consistently, a study had illustrated that higher expression of *GINS2* had significantly association with TNM stages and clinical stages.¹⁶ Above all, these findings suggested that overexpression of *GINS2* could be a novel diagnostic biomarker in lung adenocarcinoma.

The previous study had indicated that *GINS2* acted on PI3K/Akt and MEK/ERK pathways to regulate NSCLC cells proliferation, migration and invasion.¹⁶ In our study, GSEA results showed that *GINS2* may be enriched in G2M_checkpoint, E2F_targets, DNA-repair and MYC_targets_V2 pathways. Researchers have reported that G2M_checkpoint plays a crucial role in various human tumors.^{17,18} For example, G2M_checkpoint participated in regulating cells growth and apoptosis of ovarian tumor,¹⁹ colon cancer,²⁰ hepatocellular carcinoma,²¹ and breast cancer.²² Similarly, E2F_targets,^{23–25} DNA-repair^{26–28} and MYC_targets_V2^{29–31} pathways were found to participate in tumor therapy, drug resistance, immune evasion and progression. These results further supported that *GINS2* participated in the initiation and progression of lung adenocarcinoma.

We found *GINS2* to be significantly over expressed in lung adenocarcinoma cells in vitro. MTS results demonstrated that *GINS2* accelerated proliferation of tumor cells which is consistent with a previous report.¹⁶ In addition, the number of migration cells with higher expression of *GINS2* was significantly increased. Consistent with the GSEA results, we indicated that *GINS2* promoted the growth and migration abilities of tumor cells in lung adenocarcinoma. The apoptotic rate of cells transfected with *GINS2* overexpression plasmids was significantly lower than blank and NC, proving that *GINS2*

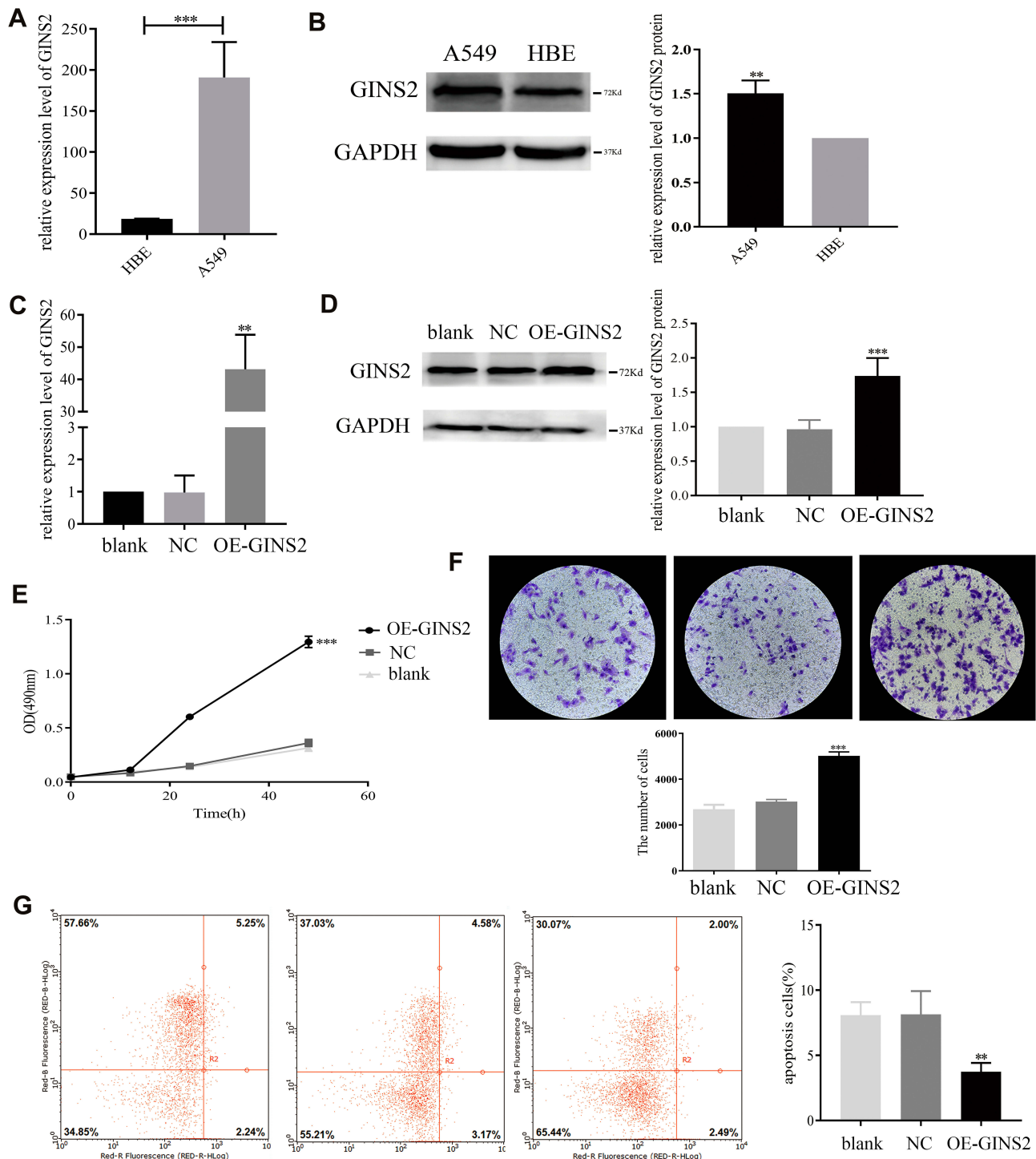


Figure 4 Biological mechanism of *GINS2* in lung adenocarcinoma. **(A)** *GINS2* mRNA expression in HBE and A549 cells. **(B)** *GINS2* protein expression in HBE and A549 cells. **(C)** *GINS2* mRNA expression in cells transfected with blank, NC and OE-*GINS2*. **(D)** *GINS2* protein expression in cells transfected with blank, NC and OE-*GINS2*. **(E)** up-regulation of *GINS2* promoted tumor cells growth. **(F)** overexpression of *GINS2* promoted tumor cells migration. **(G)** up-regulation of *GINS2* suppressed tumor cells apoptosis. ** $p < 0.01$, *** $p < 0.001$.

inactivated tumor cells apoptosis. Consistent with the previous study,¹⁶ these results further imply that *GINS2* could accelerate tumor cell proliferation and migration and inhibit tumor cells apoptosis in vitro.

In conclusion, we utilized GEO raw data to construct WGCNA co-expression network. A hub gene was identified based on the score of PPI network. High expression of *GINS2* had better diagnostic values in lung adenocarcinoma. GSEA

results predicted pathways which *GINS2* may be involved in the progress and development of lung adenocarcinoma. Moreover, we found that *GINS2* promoted the proliferation and migration of tumor cells and suppressed the apoptotic rates of tumor cells, further indicating that *GINS2* could function as a novel diagnostic and therapeutic biomarker in lung adenocarcinoma.

Abbreviations

AUC, area under curve; Ct, cycle threshold; DEG, differently expressed gene; EDTA, ethylene diamine tetraacetic acid; FBS, fetal calf serum; FCM, flow cytometry; GEO, gene expression omnibus; GSEA, gene set enrichment analysis; KEGG, Kyoto Encyclopedia of Genes and Genomes; LUAD, lung adenocarcinoma; NSCLC, non-small cell lung cancer; OD, optical density; OS, overall survival; PPI, protein-protein interaction; PVDF, polyvinylidene fluoride; ROC, receiver operating characteristic curve; TCGA, The Cancer Genome Atlas; WGCNA, weighted gene co-expression network analysis.

Funding

This study was funded by the National Natural Science Foundation of the People's Republic of China (81602923).

Disclosure

The authors report no conflicts of interest in this work.

References

- Torre LA, Bray F, Siegel RL, Ferlay J, Lortet-Tieulent J, Jemal A. Global cancer statistics, 2012. *CA Cancer J Clin*. 2015;65(2):87–108. doi:10.3322/caac.21262
- Yerukala Sathipati S, Ho SY. Identifying the miRNA signature associated with survival time in patients with lung adenocarcinoma using miRNA expression profiles. *Sci Rep*. 2017;7(1):7507. doi:10.1038/s41598-017-07739-y
- Spiro SG, Tanner NT, Silvestri GA, et al. Lung cancer: progress in diagnosis, staging and therapy. *Respirology*. 2010;15(1):44–50. doi:10.1111/j.1440-1843.2009.01674.x
- Kubota Y, Takase Y, Komori Y, et al. A novel ring-like complex of Xenopus proteins essential for the initiation of DNA replication. *Genes Dev*. 2003;17(9):1141–1152. doi:10.1101/gad.1070003
- Zhang X, Zhong L, Liu BZ, Gao YJ, Gao YM, Hu XX. Effect of *GINS2* on proliferation and apoptosis in leukemic cell line. *Int J Med Sci*. 2013;10(12):1795–1804. doi:10.7150/ijms.7025
- Rantala JK, Edgren H, Lehtinen L, et al. Integrative functional genomics analysis of sustained polyploidy phenotypes in breast cancer cells identifies an oncogenic profile for *GINS2*. *Neoplasia*. 2010;12(11):877–888. doi:10.1593/neo.10548
- Thomassen M, Jochumsen KM, Mogensen O, Tan Q, Kruse TA. Gene expression meta-analysis identifies chromosomal regions involved in ovarian cancer survival. *Genes Chromosomes Cancer*. 2009;48(8):711–724. doi:10.1002/gcc.20676
- Zheng M, Zhou Y, Yang X, et al. High *GINS2* transcript level predicts poor prognosis and correlates with high histological grade and endocrine therapy resistance through mammary cancer stem cells in breast cancer patients. *Breast Cancer Res Treat*. 2014;148(2):423–436. doi:10.1007/s10549-014-3172-7
- Liu M, Pan H, Zhang F, et al. Identification of TNM stage-specific genes in lung adenocarcinoma by genome-wide expression profiling. *Oncol Lett*. 2013;6(3):763–768. doi:10.3892/ol.2013.1469
- Grobner SN, Worst BC, Weischenfeldt J, et al. The landscape of genomic alterations across childhood cancers. *Nature*. 2018;555(7696):321–327. doi:10.1038/nature25480
- Zhai X, Xue Q, Liu Q, Guo Y, Chen Z. Colon cancer recurrence-associated genes revealed by WGCNA coexpression network analysis. *Mol Med Rep*. 2017;16(5):6499–6505. doi:10.3892/mmr.2017.7412
- Kamada K, Kubota Y, Arata T, Shindo Y, Hanaoka F. Structure of the human *GINS* complex and its assembly and functional interface in replication initiation. *Nat Struct Mol Biol*. 2007;14(5):388–396. doi:10.1038/nsmb1231
- Ye Y, Song Y-N, He S-F, Zhuang J-H, Wang G-Y, Xia W. *GINS2* promotes cell proliferation and inhibits cell apoptosis in thyroid cancer by regulating *CITED2* and *LOXL2*. *Cancer Gene Ther*. 2018;26.
- Barkley LR, Song IY, Zou Y, Vaziri C. Reduced expression of *GINS* complex members induces hallmarks of pre-malignancy in primary untransformed human cells. *Cell Cycle*. 2009;8(10):1577–1588. doi:10.4161/cc.8.10.8535
- Fei O, Liu J, Xia M, et al. *GINS2* is a novel prognostic biomarker and promotes tumor progression in early-stage cervical cancer. *Oncol Rep*. 2017;37(5):2652–2662. doi:10.3892/or.2017.5573
- Liu X, Sun L, Zhang S, Zhang S, Li W. *GINS2* facilitates epithelial-to-mesenchymal transition in non-small-cell lung cancer through modulating PI3K/Akt and MEK/ERK signaling. *J Cell Physiol*. 2019. doi:10.1002/jcp.29381
- Charrier-Savournin FB, Chateau MT, Gire V, Sedivy J, Piette J, Dulic V. p21-Mediated nuclear retention of cyclin B1-Cdk1 in response to genotoxic stress. *Mol Biol Cell*. 2004;15(9):3965–3976. doi:10.1091/mbc.e03-12-0871
- Evan GI, Vousden KH. Proliferation, cell cycle and apoptosis in cancer. *Nature*. 2001;411(6835):342–348. doi:10.1038/35077213
- Zaffaroni N, De Marco C, Villa R, Riboldi S, Daidone MG, Double JA. Cell growth inhibition, G2M cell cycle arrest and apoptosis induced by the imidazoacridinone C1311 in human tumour cell lines. *Eur J Cancer*. 2001;37(15):1953–1962. doi:10.1016/S0959-8049(01)00227-1
- Yang D, Zhang X, Zhang W, Rengarajan T. Vcenin-2 inhibits Wnt/beta-catenin signaling and induces apoptosis in HT-29 human colon cancer cell line. *Drug Des Devel Ther*. 2018;12:1303–1310. doi:10.2147/DDDT.S149307
- Luo Q, Li Y, Deng J, Zhang Z. PARP-1 inhibitor sensitizes arsenic trioxide in hepatocellular carcinoma cells via abrogation of G2/M checkpoint and suppression of DNA damage repair. *Chem Biol Interact*. 2015;226:12–22. doi:10.1016/j.cbi.2014.12.007
- He J, Chen Y, Cai L, Li Z, Guo X. UBAP2L silencing inhibits cell proliferation and G2/M phase transition in breast cancer. *Breast Cancer*. 2018;25(2):224–232. doi:10.1007/s12282-017-0820-x
- De Meyer T, Bijsmans IT, Van de Vijver KK, et al. E2Fs mediate a fundamental cell-cycle deregulation in high-grade serous ovarian carcinomas. *J Pathol*. 2009;217(1):14–20. doi:10.1002/path.2452
- Li Y, Jiao Y, Fu Z, Luo Z, Su J, Li Y. High miR-454-3p expression predicts poor prognosis in hepatocellular carcinoma. *Cancer Manag Res*. 2019;11:2795–2802. doi:10.2147/CMAR.S196655
- Ma Y, Kurtyka CA, Boyapalle S, et al. A small-molecule E2F inhibitor blocks growth in a melanoma culture model. *Cancer Res*. 2008;68(15):6292–6299. doi:10.1158/0008-5472.CAN-08-0121

26. Shah AP, Patel CN, Sureja DK, Sanghavi KP. A review on DNA repair inhibition by PARP inhibitors in cancer therapy. *Folia Med (Plovdiv)*. 2018;60(1):39–47. doi:10.1515/folmed-2017-0067
27. Mladenov E, Magin S, Soni A, Iliakis G. DNA double-strand-break repair in higher eukaryotes and its role in genomic instability and cancer: cell cycle and proliferation-dependent regulation. *Semin Cancer Biol*. 2016;37–38:51–64. doi:10.1016/j.semcancer.2016.03.003
28. Truini A, Germano G, Bardelli A. Inactivation of DNA repair-prospects for boosting cancer immune surveillance. *Genome Med*. 2018;10(1):91. doi:10.1186/s13073-018-0603-9
29. Dang CV. MYC on the path to cancer. *Cell*. 2012;149(1):22–35. doi:10.1016/j.cell.2012.03.003
30. Stine ZE, Walton ZE, Altman BJ, Hsieh AL, Dang CV. MYC, metabolism, and cancer. *Cancer Discov*. 2015;5(10):1024–1039. doi:10.1158/2159-8290.CD-15-0507
31. Hsieh AL, Walton ZE, Altman BJ, Stine ZE, Dang CV. MYC and metabolism on the path to cancer. *Semin Cell Dev Biol*. 2015;43:11–21. doi:10.1016/j.semcdb.2015.08.003

OncoTargets and Therapy

Dovepress

Publish your work in this journal

OncoTargets and Therapy is an international, peer-reviewed, open access journal focusing on the pathological basis of all cancers, potential targets for therapy and treatment protocols employed to improve the management of cancer patients. The journal also focuses on the impact of management programs and new therapeutic

agents and protocols on patient perspectives such as quality of life, adherence and satisfaction. The manuscript management system is completely online and includes a very quick and fair peer-review system, which is all easy to use. Visit <http://www.dovepress.com/testimonials.php> to read real quotes from published authors.

Submit your manuscript here: <https://www.dovepress.com/oncotargets-and-therapy-journal>